A Dual-Polarized 1-D Tightly Coupled Dipole Array Antenna

Hakjune Lee and Sangwook Nam, *Senior Member, IEEE*

***Abstract*— A dual-polarized 1-D tightly coupled dipole array (TCDA) antenna is proposed in this paper. To apply the TCDA design concept to a 1-D array, we place a conducting wall with slits and ferrite sheets along the 1-D dipole array. The simulated dual-polarized 1-D infinite TCDA antenna has a wide overlapped bandwidth of 2.83:1 (from 1 to 2.83 GHz) with VSWR < 2, high isolation (>25 dB) between the horizontal and vertical polarizations (VPs), and low height of 1/5 λ at the lowest operating frequency. A prototype of the proposed array is fabricated and measured, which consists of nine horizontal polarization (HP) dipoles and eight VP dipoles interleaved between the HP dipoles. The measured results show high gains >7.2 dB when scanning up to 30° and a wide half-power beamwidth in the *yz* plane >61° over the operating frequency band for both polarizations, consistent with the simulation result.**

***Index Terms*— Array antennas, base station, dual-polarized antenna, phased array.**

I. Introduction

DUAL-POLARIZED wideband array antennas are widely used for many applications such as mobile communication, radars, and electric warfare. The dual-polarized array should have the following characteristics: 1) horizontal and vertical polarization (VP) diversity with high isolation between them; 2) wide bandwidth for covering the many frequency bands; and 3) low profile for compact array size [1]. These issues have been studied by various types of array antennas [2]–[14].

The tapered slot array (TSA) or the Vivaldi array, which is a traveling wave antenna, is a well-known wideband array antenna [15]. The TSA can have a wide bandwidth and high gain, but it has a high height and a large cross-polarization radiation when scanning [2]–[4].

Tightly coupled dipole array (TCDA) is one of the wideband and low-profile array antennas proposed by Munk [5]. Recently, various types of TCDAs, which have wide bandwidths of 5:1 [6], 3:1 [7], 6.9:1 [8], and 6:1 [9], have been developed. They also have wide scan angle $\leq 45°$ for [6]–[8] and $\leq 60°$ for [9] with mitigated impedance matching criteria and a low-profile of less than 1/5 λ_{low}. Up to date, the TCDAs have been designed in the 2-D array, giving a pencil beam pattern.

However, wideband and low-profile 1-D arrays are needed in several applications such as base station antennas. As a result, many dual-polarized base station antennas with extended bandwidths and low-profiles were proposed [10]–[15]. However, the bandwidths of the antennas were limited to 23.7% with 1/4 λ_{low} height [10], 45% with 1/5.48 λ_{low} [11], 57.8% with 1/4.4 λ_{low} height [12], and 27.8% with 1/4.92 λ_{low} height [15].

In this paper, we propose a dual-polarized 1-D TCDA antenna by simulating the 2-D TCDA operation condition with proper sidewall. The designed 1-D TCDA has scan angle up to ±30°, a height of 1/5 λ_{low}, and the bandwidth of 2.83:1 for both polarizations when it radiates broadside.

This paper is organized as follows. In Section II, TCDA theory is briefly explained. Section III shows the configuration of the proposed array antenna with its operating principle. The effects of the parameters of the side structure are also provided. Section IV presents the fabrication of the 1-D TCDA antenna and measured results. The conclusion is given in Section V.

II. Theory of the TCDA

In this section, we briefly explain the operating principle of TCDA, before introducing the proposed dual polarized 1-D TCDA antenna. Although the TCDA theory is based on the 2-D periodic array, it gives the insight of the 1-D periodic TCDA design.

In 2003, Munk [5] proposed the TCDA concept which is based on Wheeler's [18] current sheet array. TCDA is an infinite 2-D array on the ground plane as shown in Fig. 1(a). The properties of an infinite 2-D periodic TCDA can be equivalent to those of a unit dipole in a virtual waveguide, which is presented in Fig. 1(b). The virtual waveguide consists of the perfect magnetic conductor (PMC) boundary parallel to the dipole direction and the perfect electric conductor (PEC) boundary perpendicular to the dipole direction. The transverse electromagnetic (TEM) mode can exist in the waveguide because of this particular boundary condition. Therefore, the waveguide can be regarded as a transmission line, and its characteristic impedance and wavenumber are given by [18]

$$Z_c = \frac{a}{b}\sqrt{\frac{\mu}{\varepsilon}} \tag{1}$$

$$k = \omega\sqrt{\mu\varepsilon} \tag{2}$$

Manuscript received January 28, 2017; revised May 4, 2017; accepted June 7, 2017. Date of publication July 4, 2017; date of current version September 1, 2017. This work was supported by the Center for Advanced Meta-Material funded by the Ministry of Science, ICT, and Future Planning as Global Frontier Project under Grant CAMM-2014M3A6B3063708. *(Corresponding author: Sangwook Nam.)*

H. Lee is with the Electronics and Telecommunications Research Institute, Daejeon 34129, South Korea (e-mail: hakzoon@etri.re.kr).

S. Nam is with the Institute of New Media Communication, School of Electrical and Computer Engineering, Seoul National University, Seoul 151-742, South Korea (e-mail: snam@snu.ac.kr).

Color versions of one or more of the figures in this paper are available online at http://ieeexplore.ieee.org.

Digital Object Identifier 10.1109/TAP.2017.2723262

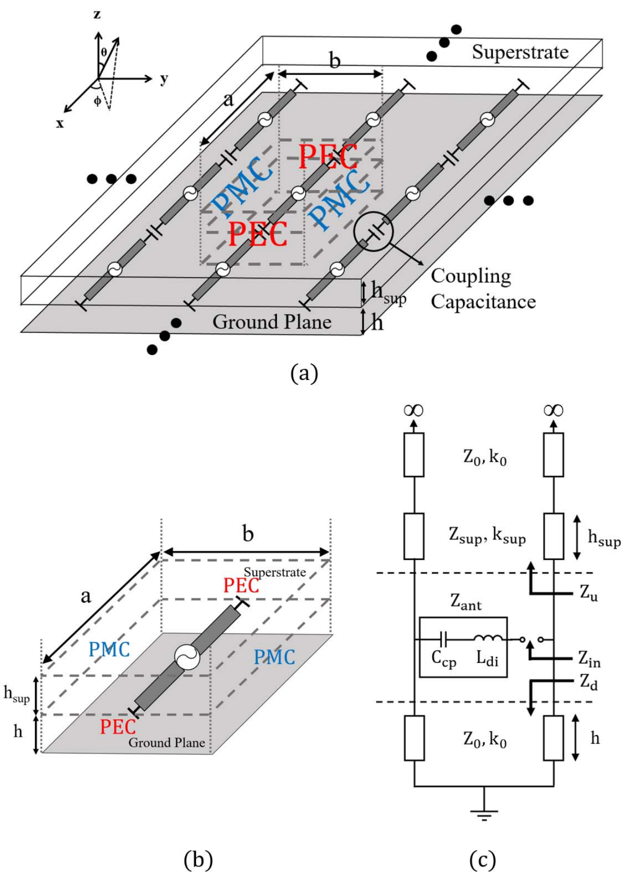

Fig. 1. (a) Sketch of an infinite TCDA including a ground plane and a superstrate. (b) Unit cell of the TCDA. (b) Equivalent circuit of the TCDA (TEM mode).

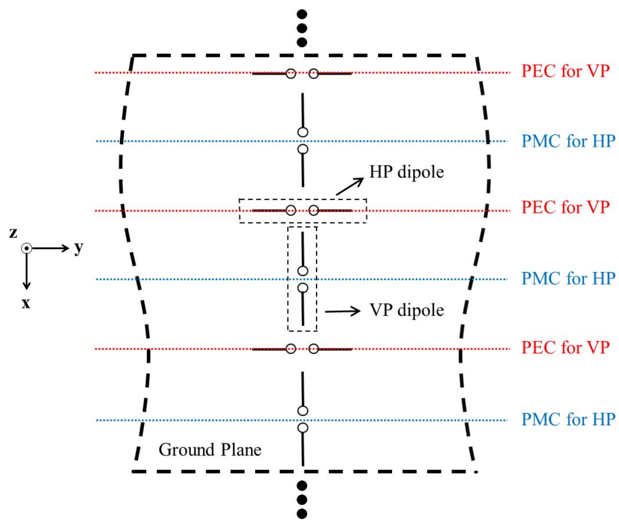

Fig. 2. Schematic of the 1-D truncated dual-polarized TCDA.

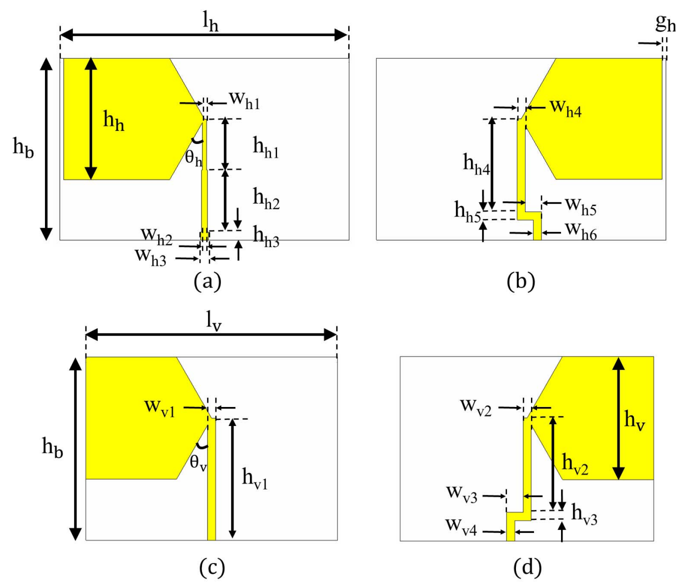

Fig. 3. Configuration of dipoles for both polarizations. (not scaled) (a) Front side of the HP dipole. (b) Back side of the HP dipole. (c) Front side of the VP dipole. (d) Back side of the VP dipole. (h_b = 45, l_h = 72, g_h = 1, h_h = 30, h_{h1} = 12.6, h_{h2} = 15.4, h_{h3} = 2, h_{h4} = 28, h_{h5} = 1, w_{h1} = 0.5, w_{h2} = 0.7, w_{h3} = 1, w_{h4} = 0.5, w_{h5} = 1, w_{h6} = 0.5, θ_h = 30, l_v = 62, h_v = 30, h_{v1} = 30, h_{v2} = 28, h_{v3} = 1, w_{v1} = 1, w_{v2} = 0.5, w_{v3} = 1, w_{v4} = 0.5, and θ_v = 30. Units: mm; degree for parameter θ_h, θ_v only.)

where ε is the permittivity of the material inside the waveguide, and μ is the permeability of the material inside the waveguide.

Munk also proposed a simple equivalent circuit of the TCDA as shown in Fig. 1(c). The characteristic impedances of the transmission line Z_0 and Z_{sup} are determined by (1). Likewise, the wavenumber k_0 and k_{sup} are determined by (2). The C_{cp} and L_{di} are coupling capacitance between the neighboring dipoles in close proximity and inductance of the dipole, respectively. The TCDA can have a wide bandwidth and low profile, because input impedance, $Z_{\text{in}} = Z_u // Z_d + Z_{\text{ant}}$, can have improved impedance matching in wideband that starts at low frequency. Especially, the C_{cp} can compensate the inductance looking into the ground plane Z_d.

III. Design of the Dual Polarized 1-D TCDA

All TCDAs have been previously studied and implemented in a 2-D structure. However, there are several applications that need 1-D arrays which have wideband and low-profile characteristics. In order to design such a 1-D array, which is based on the operation principle of 2-D TCDA, we use a conducting wall with slits and ferrite sheets for a dual-polarized 1-D TCDA with fan beam radiation pattern. A detailed explanation is given in the following sections.

A. Antenna Structure and Operating Principle

Let both polarization dipoles be arranged in the x-direction, as shown in Fig. 2. Then, the PEC boundary conditions for VP and the PMC boundary conditions for horizontal polarization (HP) are inherently given, as shown in Fig. 2 (dotted red and blue lines). As the boundary conditions on both sides of the dipoles are open boundaries, additional side structures are required on both sides of the dipole to maintain the 2-D TCDA boundary conditions as shown in Fig. 1(a) and (b).

Fig. 3(a) and (b) shows the front and back sides of printed circuit board (PCB) of the designed HP dipole. Also, those of the VP dipole PCB are shown in Fig. 3(c) and (d). The Rogers

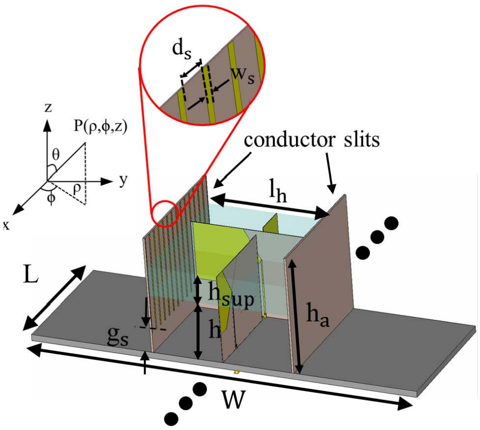

(a)

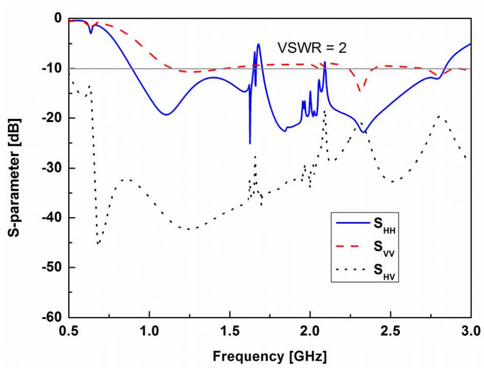

(b)

Fig. 4. Dual-polarized 1-D TCDA with a conducting wall with slits. (a) Antenna structure. (b) S-parameter response. (not scaled) ($L = 70$, $W = 200$, $h = 30$, $h_{\text{sup}} = 15$, $g_s = 0.3$, $h_a = 60$, $w_s = 1$, and $d_s = 4$. Units: mm.)

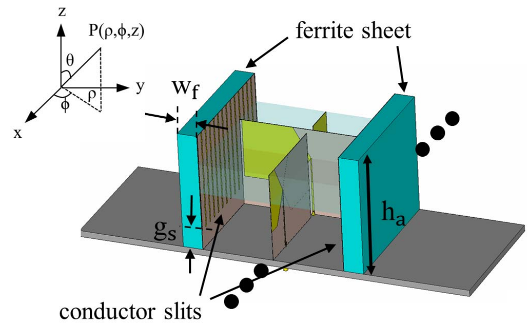

(a)

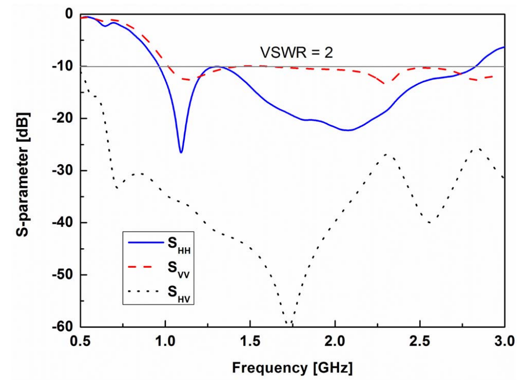

(b)

Fig. 5. Proposed dual-polarized 1D TCDA with conducting walls with slits and ferrite sheets. (a) Antenna structure. (b) S-parameter response. (not scaled) ($g_s = 0.3$, $h_a = 60$, $w_f = 1$. Units: mm.)

RT/Duroid 5880 with a thickness of 0.254 mm, dielectric constant of 2.2, and dielectric loss tangent of 0.001 are used as a substrate for both polarization dipoles. The unbalanced feed lines are used: the feeding lines on the front side of both polarizations are connected to the SubMiniature version A (SMA) connector directly, and the feeding lines on the back side of both polarizations are connected to the ground plane.

Fig. 4(a) shows the 1-D TCDA arranged in the x-direction with side walls using vertically standing copper slits only. The element spacing L is determined by the grating lobe formula

$$L = \frac{c}{f_{\text{hi}}(1 + \sin\theta_s)} \tag{3}$$

where the highest operating frequency f_{hi} is 2.83 GHz, the maximum scan angle θ_s is 30°, and then, L is 70 mm. The polytetrafluoroethylene (PTFE) with a dielectric constant of 2.1 and dielectric loss tangent of 0.0 005 is used as the superstrate. The FR-4 with a thickness of 0.2 mm, dielectric constant of 4.3, and dielectric loss tangent of 0.025 is used as the dielectric board of the copper strips. The dielectric board stands vertically from the ground plane to h_a height. The copper strips, the width, and the distance between the neighboring strips of which are w_s and d_s, respectively, are separated from the ground plane by g_s, and its height is h_a. The boundaries parallel to the x-direction operate as a PEC because the vertically standing copper strips are parallel to the electric field of the HP. The S-parameter response of the HP as shown in Fig. 4(b) shows a wide impedance matching starting from 0.9 GHz. However, the multiple resonances, which are magnetic coupling resonances between the strips, occur within the bandwidth. For the VP, the gap capacitance between the neighboring elements cancels the inductive reactance of the ground plane at a low frequency. The impedance is matched from 1.1 GHz. Therefore, the side wall with conducting slit cannot only satisfy the required boundary conditions for TCDA operation.

In order to implement the required side wall boundary conditions for dual-polarized 1-D TCDA, a conducting wall with slits and ferrite sheet is proposed as shown in Fig. 5(a). The conducting wall with slits is as described above, and the ferrite sheet with a thickness of w_f and height of h_a is modeled by Fair-Rite Products Corp. M1 material. The S-parameter simulation result of the proposed array is shown in Fig. 5(b). For HP, the many magnetic coupling resonances between the strips disappear unlike in the 1-D TCDA with slits only. This is due to the decrease of the coupling between the strips by the ferrite sheet: the large loss of the ferrite sheet at the magnetic coupling resonance frequencies makes the Q-factors of the resonances become lower. As a result, the magnetic coupling resonances are disappeared. The impedance matching of HP is performed from 0.96 to 2.83 GHz. For the VP, the ferrite sheets provide high wave impedance as

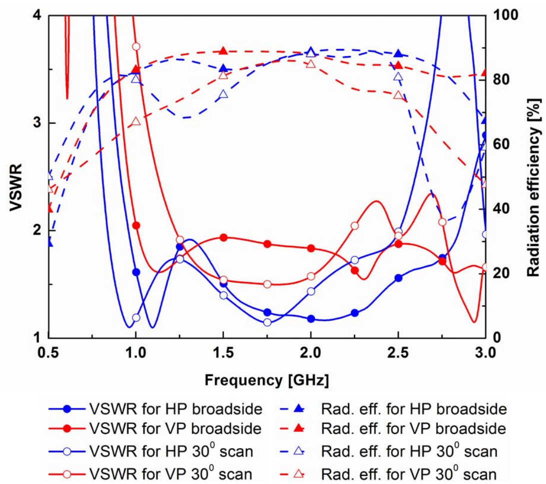

Fig. 6. VSWR and radiation efficiency for both polarizations when the array radiates at broadside and 30° scanning directions.

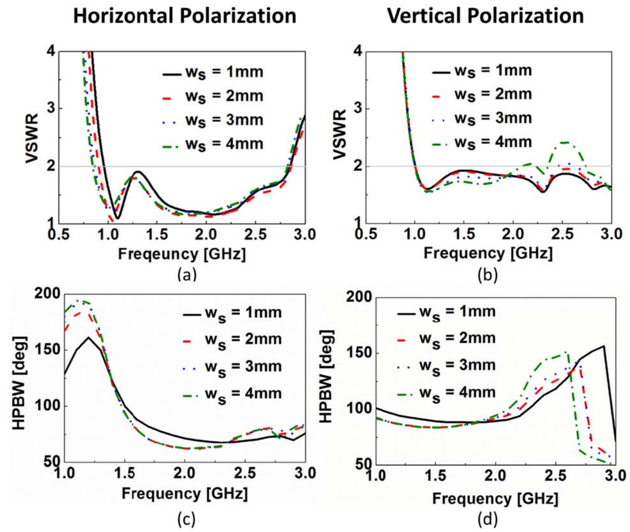

Fig. 7. VSWR variations according to the (a) w_s for HP, (b) w_s for VP, (c) g_s for HP, (d) g_s for VP, (e) h_a for HP, and (f) h_a for VP.

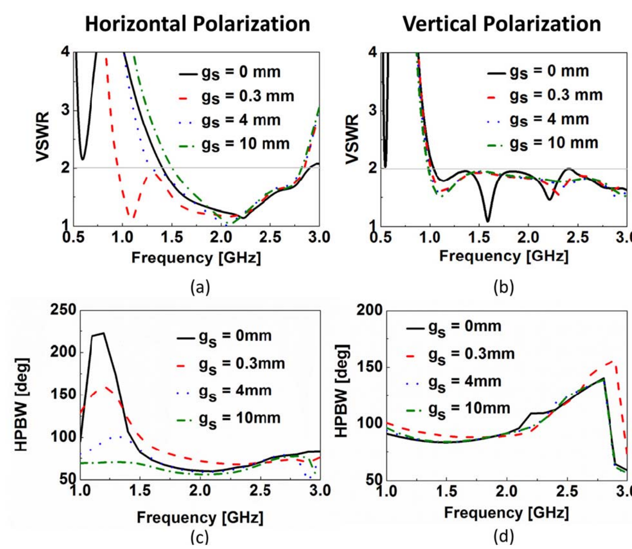

Fig. 8. Variations of VSWR and HPBW in the yz plane according to the g_s. (a) VSWR for HP. (b) VSWR for VP. (c) HPBW for HP. (d) HPBW for VP.

a PMC boundary. Consequently, the impedance matching of the VP is extended toward the low frequency unlike in the 1-D TCDA with a conducting wall with slits. The overlapped bandwidth is 2.83:1 (from 1 to 2.83 GHz) with VSWR ≤ 2. The isolation between the HP and VP ports is greater than 25 dB in the frequency band.

Fig. 6 shows the VSWR and radiation efficiency of the proposed 1-D TCDA for both polarizations when the array radiates to the broadside (0°) and 30° scanned directions in the xz plane. When the proposed array radiates to the broadside, radiation efficiency is greater than 81%. When the array radiates to the 30° scanned direction, the overlapped bandwidth decreases to 2.2:1 (from 1.16 to 2.57 GHz) with VSWR < 2.3 and radiation efficiency $>70\%$. The VSWR and radiation efficiency when the scan angle between 0° and 30° are between the values when the scan angle is 0° and 30°, respectively.

B. Side Structure Parametric Study

Like optimizing the antenna or feeding line parameters for a wideband and a low profile in 2-D TCDA [6]–[9], we investigate the sidewall structure to understand its effect on the performance of 1-D TCDA.

The effects of the width of the strip (w_s) on VSWR are presented in Fig. 7(a) and (b). Let the distance between the center of the strips and the center of the adjacent strip be fixed at 5 mm ($w_s + d_s = 5$ mm). As w_s increases, the bandwidth of the HP extends slightly toward the low frequencies, and the impedance matching of the VP becomes worse at a high frequency because the wide strips operate more like PEC for both polarizations. For the HP, the wider strips provide the PEC–PMC boundaries, so that the return loss improves at a low frequency. For the VP, as the width of the strip increases, the impedance matching deteriorates because of the increasing influence of the conductor at high frequencies. The HPBWs in the yz plane are also affected w_s and are shown in Fig. 7(c) and (d). The half-power beamwidth (HPBW) increases for both polarizations when the w_s increases.

The effects of the distance from the ground plane to slits (g_s) on VSWR are presented in Fig. 8(a) and (b). When the slits come in contact with the ground plane ($g_s = 0$ mm), the bandwidth of HP decreases at low frequencies. Increasing the g_s causes the electromagnetic field to leak, thus negatively affecting the input matching at low frequencies. The VSWR of the VP does not change because the copper strip does not affect the VP. The HPBWs in the yz plane according to g_s are shown in Fig. 8(c) and (d). When g_s increases, the maximum value of the HPBW decreases for HP at the low frequency. For VP, the HPBW is hardly influenced.

The effects of the side structure height (h_a) on VSWR are presented in Fig. 9(a) and (b). If h_a increases, the boundaries parallel to the x-direction will behave more like the 2-D TCDA boundaries. As h_a increases, the input matching of the HP becomes possible from a low frequency to a high frequency, and the input matching of the VP is slightly improved.

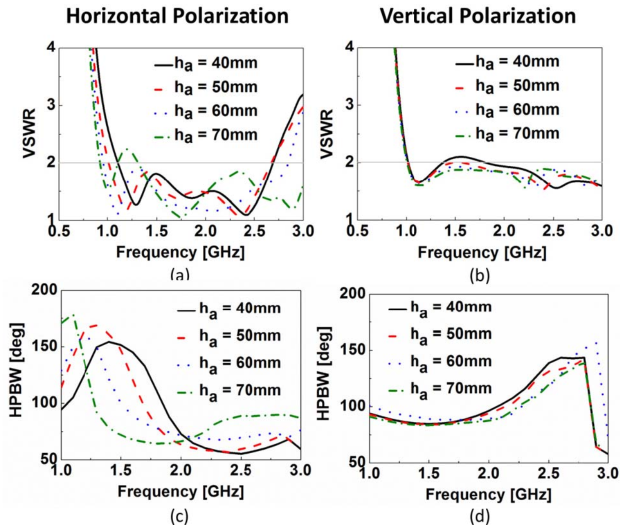

Fig. 9. Variations of VSWR and HPBW in the yz plane according to the h_a. (a) VSWR for HP. (b) VSWR for VP. (c) HPBW for HP. (d) HPBW for VP.

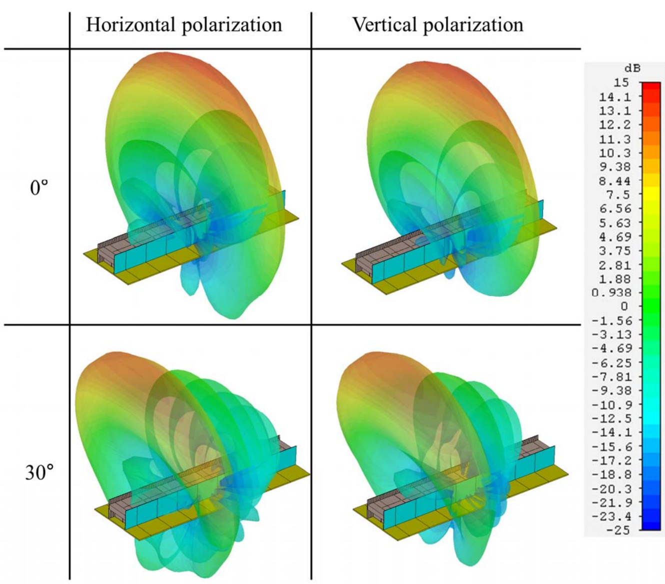

Fig. 10. 3-D radiation pattern (broadside and 30° scan) of fully simulated proposed array antenna prototype at 1.75 GHz for both polarizations.

Choosing the lowest height that can cover the desired frequency band is reasonable, and therefore we choose $h_a = 60$ mm. The HPBWs in the yz plane according to h_a are shown in Fig. 9(c) and (d). As h_a increases, the maximum HPBW frequency is lowered. The HPBW of VP at high frequency slightly increases with increasing h_a.

Fig. 10 shows the fully simulated 3-D pattern of the proposed array antenna prototype at 1.75 GHz. The total array antenna which is identically fabricated is simulated, and the radiation pattern is fan beam which can move from broadside (0°) to forward or backward direction (30°).

IV. Prototype of the Proposed 1-D TCDA and Measurement Results

A. Fabrication

A prototype of the proposed 1-D TCDA which consists of 1×9 HP dipoles and 1×8 VP dipoles is implemented as shown in Fig. 11. For the symmetry of the array, nine HP dipoles are used and eight VP dipoles are placed between the HP dipoles. The array prototype is constructed on a 600 mm $\times$ 200 mm, 0.12 m^2 aluminum plate. On the aluminum plate, the FR-4 substrate which has a thickness of 0.2 mm, a half ounce of copper cladding on both sides, and the same size of the aluminum plate is used for soldering dipoles and ground planes. First, the dipoles of both polarizations are soldered onto the SMA connector and the FR-4 substrate at each feeding spot. The spacers are fixed on the ground plane using nylon screws, and then the superstrates were fixed on the spacers using the screws. As mentioned above, the superstrate is implemented by blocks of PTFE ($\varepsilon_r = 2.1$) which has a thickness of 15 mm. To complete the prototype, additional PTFE blocks are used at the ends of the array. Finally, the side structures are placed and fixed on both sides of the dipoles.

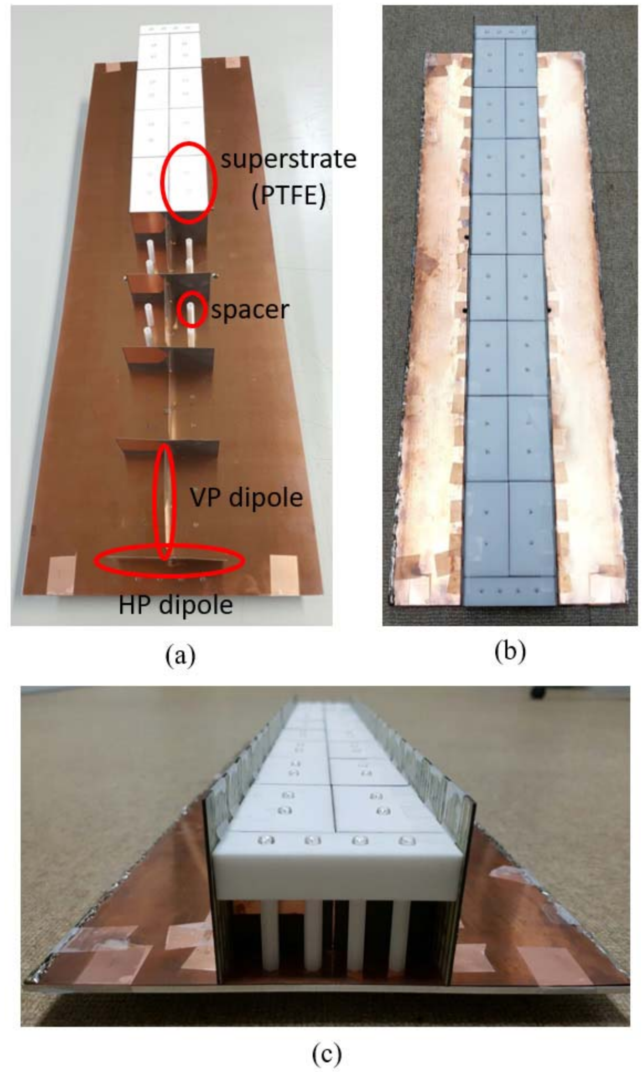

Fig. 11. (a) Prototype at three stages of fabrication. (b) Top view of the implemented 1-D TCDA prototype. (c) Front view of the prototype.

B. Measurement Results

The radiation pattern of the array prototype is measured in the anechoic chamber. The measurement process is based on the unit excitation active element pattern method [20].

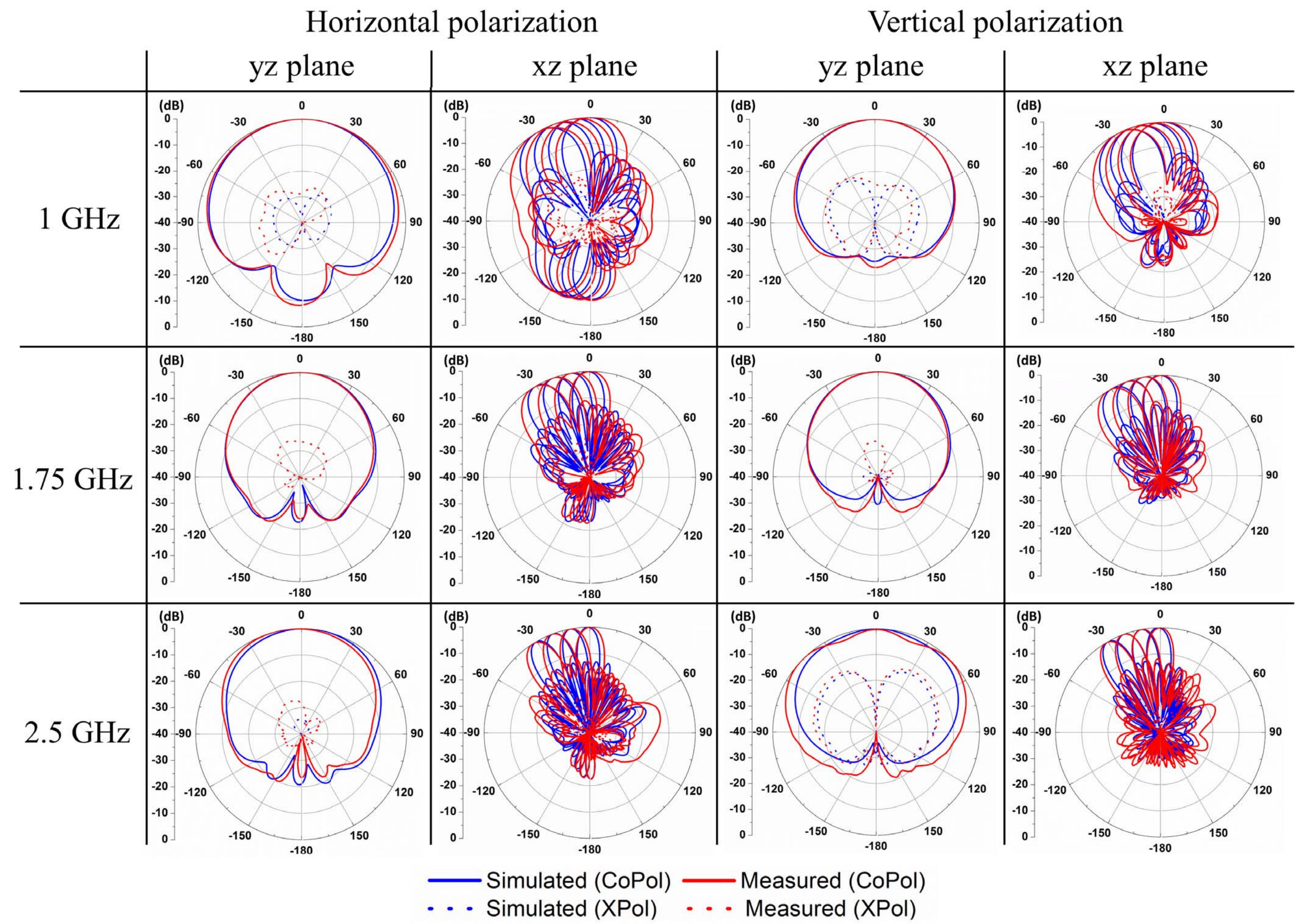

Fig. 12. Simulated and measured radiation patterns of the prototype array.

TABLE I
COMPARISON OF THE PERFORMANCES FOR THE PROPOSED AND REFERENCE ANTENNAS

Ref	Dimension (mm)	Bandwidth	Height (λ_{low})	Isolation (dB)	HPBW in the yz plane (°)	Gain (dBi)	Array (scan angle)
[10]	130 × 130	1.71 ~ 2.17 GHz (23.7 %)	1 / 4	> 34	~ 70	> 8	No
[11]	280 × 280	1.71 ~ 2.72 GHz (45.6 %)	1 / 5.48	> 30	NG	> 8.9	No
[12]	NG	1.6 ~ 2.9 GHz (57.8 %)	1 / 4.4	~ 30	65 ± 10	> 15.5	8-element (No scan)
[13]	360 × 280 700 × 280	1.54 ~ 2.86 GHz (60.0 %) 1.47 ~ 3.00 GHz (68.4 %)	1 / 4.32 1 / 4.54	NG	95 ± 5	~ 8 ~14	8-element (No scan)
[14]	140 × 140 600 × 140	1.70 ~ 2.70 GHz (45.5 %)	1 / 5.07	> 25	68 ± 2 66.56 ± 2.22	~8.2 ~14.5	5-element (8°)
[15]	140 × 140 1370 × 140	1.7 ~ 2.25 GHz (27.8 %)	1 / 4.92	> 25 > 30	66.3 ± 2.9 65 ± 5	> 8 > 15.8	10-element (8°)
This work	600 × 200	1 ~ 2.83 GHz (95.6%)	1 / 5	> 25	> 61	> 8.6	9-HP element, 8-VP element (30°)

*NG: not given

According to the method, all element patterns that include mutual coupling with the surrounding array environments and the other elements are individually measured with 50-**Ω** termination at all the other ports. Then, the total number of patterns at various scan angles can be synthesized through postprocessing. The overall array E-field pattern is obtained as follows [20]:

$$\mathbf{E}(\theta, \phi) = \sum_{i=1}^{N} V_i \mathbf{g}_i(\theta, \phi) \tag{4}$$

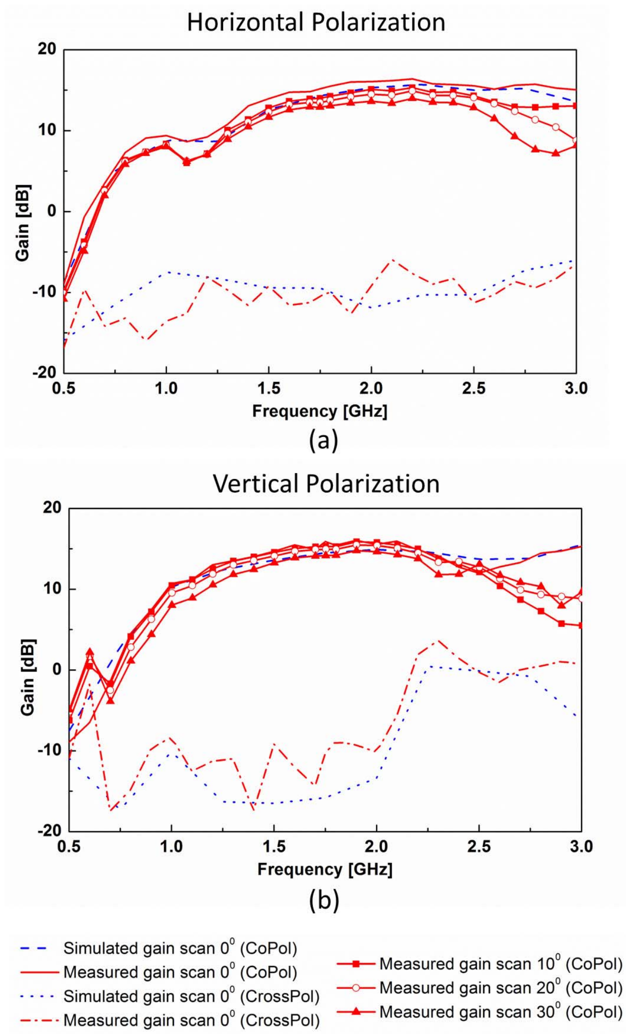

Fig. 13. Simulated and measured broadside gain of the prototype array. (a) HP. (b) VP.

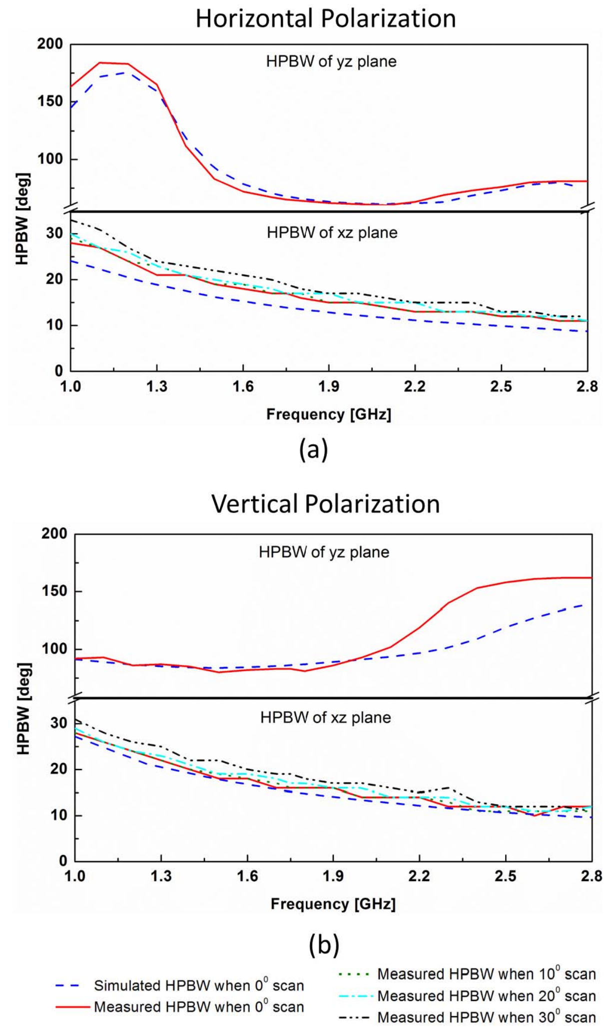

Fig. 14. Simulated and measured broadside gain of the prototype array. (a) HP. (b) VP.

where V_i is the complex-valued feed voltage applied to the ith element, N is the number of array elements, and $\mathbf{g}_i(\theta, \phi)$ is the complex-valued field pattern generated by the unit excitation of the ith element.

The normalized simulated and measured patterns at 1, 1.75, and 2.5 GHz for both polarizations are presented in Fig. 12. The measured patterns are in good agreement with the simulated patterns. The radiation pattern of the prototype array antenna has a wide beamwidth in the yz plane with a low cross-polarization level less than -10 dB for both polarizations. The xz plane patterns show that the array can be scan to the desired direction in the xz plane up to 30° for both polarizations. In Fig. 12, only the downtilt patterns are presented, but the uptilt can also be possible because of the symmetric of the array. The grating lobe is not shown over the frequency range in 1–2.83 GHz for both polarizations. The front-to-back ratio is greater than 10 dB in both planes for both polarizations without any additional reflector, and it may be improved by the additional reflector [21], [22].

Fig. 13 shows the measured realized gain versus frequency. The simulated gains are obtained from the simulations of the full array that are identical to the prototype array (1×9 HP dipoles and 1×8 VP dipoles). The measured result shows a good agreement with the simulation result. When the array radiates to the broadside (0°), the array gains achieved for both polarization arrays are higher than 8.6 dB, in the operating frequency band (1–2.83 GHz). Moreover, the cross-polarized gain is greater than 10 dB below the co-polarized gain. When the array radiates to a slanted angle, a slight gain decline is observed in both polarizations. This result is in accordance with the widened beamwidth in the xz plane and the deteriorating VSWR at a large scan angle. However, the scanned gain maintains the high gain over 7.2 dB at the frequency band for both polarizations. Thus, the proposed array antenna can cover a wide scan angle over a wide bandwidth.

Fig. 14 presents the simulated and measured HPBW for both polarizations. The HPBW of the HP in the yz plane is greater than 61° and that in the xz plane is less than 33° over the frequency band. The HPBW of the VP in the yz plane is greater than 83° and that in the xz plane is less than 31° in the frequency band. At high frequencies, the measured

HPBW in the xz plane is greater than that in the simulation. The difference may be due to the effect of the current being greater than the simulation on the ground plane. As previously mentioned, the HPBW in the xz plane is broader when the scan angle is large. For both polarizations, the HPBWs in the yz plane may be stable by adding the reflector.

The overall antenna performances of our proposed antenna are compared with the reference antennas [10]–[15] are listed in Table I. The proposed antenna accomplishes a conspicuous enhancement in its bandwidth maintaining a low profile and wide scan ability.

V. Conclusion

A dual-polarized 1-D TCDA antenna using conducting walls with slits and ferrite sheets is presented in this paper. The conducting walls with slits and ferrite sheets provide a PEC boundary to the HP and a PMC boundary to the VP, so that the element in the 1-D array seems as if it is located in the 2-D TCDA structure. Moreover, the ferrite sheets alleviate the magnetic coupling resonances of the slits. Therefore, the array antenna achieves a wide overlapped bandwidth of 2.83:1 (1–2.83 GHz) with low total height of 1/5 λ_{low}, high isolation >25 dB, and large unit cell spacing of 1/1.5 λ_{high}. The prototype of the proposed 1-D array with nine HP elements and eight VP elements interleaved is implemented. The prototype shows a high gain >7.2 dB when scanning up to 30°, and a wide HPBW in the yz plane $>61°$ is observed in the operating frequency band for both polarizations. The array antenna can be used in 1-D phased array systems such as a base station array antenna.

References

[1] G. C. Tavik *et al.*, "The advanced multifunction RF concept," *IEEE Trans. Microw. Theory Techn.*, vol. 53, no. 3, pp. 1009–1020, Mar. 2005.

[2] R. W. Kindt and W. R. Pickles, "Ultrawideband all-metal flared-notch array radiator," *IEEE Trans. Antennas Propag.*, vol. 58, no. 11, pp. 3568–3575, Nov. 2010.

[3] Y. Zhang and A. K. Brown, "Bunny ear combline antennas for compact wide-band dual-polarized aperture array," *IEEE Trans. Antennas Propag.*, vol. 59, no. 8, pp. 3071–3075, Aug. 2011.

[4] J.-B. Yan, S. Gogineni, B. Camps-Raga, and J. Brozena, "A dual-polarized 2–18-GHz Vivaldi array for airborne radar measurements of snow," *IEEE Trans. Antennas Propag.*, vol. 64, no. 2, pp. 781–785, Feb. 2016.

[5] B. A. Munk, *Finite Antenna Arrays and FSS*. New York, NY, USA: Wiley, 2003.

[6] S. S. Holland and M. N. Vouvakis, "The planar ultrawideband modular antenna (PUMA) array," *IEEE Trans. Antennas Propag.*, vol. 60, no. 1, pp. 130–140, Jan. 2012.

[7] S. S. Holland, D. H. Schaubert, and M. N. Vouvakis, "A 7–21 GHz dual-polarized planar ultrawideband modular antenna (PUMA) array," *IEEE Trans. Antennas Propag.*, vol. 60, no. 10, pp. 4589–4600, Oct. 2012.

[8] J. P. Doane, K. Sertel, and J. L. Volakis, "A wideband, wide scanning tightly coupled dipole array with integrated balun (TCDA-IB)," *IEEE Trans. Antennas Propag.*, vol. 61, no. 9, pp. 4538–4548, Sep. 2013.

[9] M. H. Novak and J. L. Volakis, "Ultrawideband antennas for multiband satellite communications at UHF–Ku frequencies," *IEEE Trans. Antennas Propag.*, vol. 63, no. 4, pp. 1334–1341, Apr. 2015.

[10] A. Elsherbini, J. Wu, and K. Sarabandi, "Dual polarized wideband directional coupled sectorial loop antennas for radar and mobile base-station applications," *IEEE Trans. Antennas Propag.*, vol. 63, no. 4, pp. 1505–1513, Apr. 2015.

[11] Y. Jin and Z. Du, "Broadband dual-polarized F-probe fed stacked patch antenna for base stations," *IEEE Antennas Wireless Propag. Lett.*, vol. 14, pp. 1121–1124, 2015.

[12] Y. Cui, R. Li, and P. Wang, "A novel broadband planar antenna for 2G/3G/LTE base stations," *IEEE Trans. Antennas Propag.*, vol. 61, no. 5, pp. 2767–2774, May 2013.

[13] Y. Cui, R. Li, and P. Wang, "Novel dual-broadband planar antenna and its array for 2G/3G/LTE base stations," *IEEE Trans. Antennas Propag.*, vol. 61, no. 3, pp. 1132–1139, Mar. 2013.

[14] Q.-X. Chu, D.-L. Wen, and Y. Luo, "A broadband ±45° dual-polarized antenna with Y-shaped feeding lines," *IEEE Trans. Antennas Propag.*, vol. 63, no. 2, pp. 483–490, Feb. 2015.

[15] D.-L. Wen, D.-Z. Zheng, and Q.-X. Chu, "A dual-polarized planar antenna using four folded dipoles and its array for base stations," *IEEE Trans. Antennas Propag.*, vol. 64, no. 12, pp. 5536–5542, Dec. 2016.

[16] J. Tak and J. Choi, "A low-profile dipole array antenna with monopole-like radiation for on-body communications," *J. Electromagn. Eng. Sci.*, vol. 15, no. 4, pp. 245–249, Oct. 2015.

[17] P. J. Gibson, "The Vivaldi aerial," in *Proc. 9th Eur. Microw. Conf.*, Brighton, U.K., Sep. 1979, pp. 101–105.

[18] H. A. Wheeler, "The radiation resistance of an antenna in an infinite array or waveguide," *Proc. IRE*, vol. 36, no. 4, pp. 478–487, Apr. 1948.

[19] H. Wheeler, "Simple relations derived from a phased-array antenna made of an infinite current sheet," *IEEE Trans. Antennas Propag.*, vol. AP-13, no. 4, pp. 506–514, Jul. 1965.

[20] D. F. Kelley and W. L. Stutzman, "Array antenna pattern modeling methods that include mutual coupling effects," *IEEE Trans. Antennas Propag.*, vol. 41, no. 12, pp. 1625–1632, Dec. 1993.

[21] S. X. Ta, H. Choo, I. Park, and R. W. Ziolkowski, "Multi-band, wide-beam, circularly polarized, crossed, asymmetrically barbed dipole antennas for GPS applications," *IEEE Trans. Antennas Propag.*, vol. 61, no. 11, pp. 5771–5775, Nov. 2013.

[22] L. Zhang *et al.*, "Single-feed ultra-wideband circularly polarized antenna with enhanced front-to-back ratio," *IEEE Trans. Antennas Propag.*, vol. 64, no. 1, pp. 355–360, Jan. 2016.

Hakjune Lee received the B.S. and M.S. degrees in electrical and computer engineering from Seoul National University, Seoul, South Korea, in 2014 and 2016, respectively.

Since 2016, he has been a Researcher with the Electronics and Telecommunications Research Institute, Daejeon, South Korea. His current research interests include ultrawideband array antennas and metamaterial.

Sangwook Nam (S'87–M'88–SM'11) received the B.S. degree in electrical engineering from Seoul National University, Seoul, South Korea, in 1981, the M.S. degree in electrical engineering from the Korea Advanced Institute of Science and Technology, Seoul in 1983, and the Ph.D. degree in electrical engineering from The University of Texas at Austin, Austin, TX, USA, in 1989.

From 1983 to 1986, he was a Researcher with the Gold Star Central Research Laboratory, Seoul. Since 1990, he has been a Professor with the School of Electrical Engineering and Computer Science, Seoul National University. His current research interests include analysis/design of electromagnetic structures, antennas, and microwave active/passive circuits.